Climate Change over the Equatorial Indo-Pacific in Global Warming*

CHIE IHARA, YOCHANAN KUSHNIR, AND MARK A. CANE

Lamont-Doherty Earth Observatory, Columbia University, Palisades, New York

VICTOR H. DE LA PEÑA

Department of Statistics, Columbia University, New York, New York

(Manuscript received 14 April 2008, in final form 30 September 2008)

ABSTRACT

The response of the equatorial Indian Ocean climate to global warming is investigated using model outputs submitted to the Intergovernmental Panel on Climate Change (IPCC) Fourth Assessment Report. In all of the analyzed climate models, the SSTs in the western equatorial Indian Ocean warm more than the SSTs in the eastern equatorial Indian Ocean under global warming; the mean SST gradient across the equatorial Indian Ocean is anomalously positive to the west in a warmer twenty-first-century climate compared to the twentieth-century climate, and it is dynamically consistent with the anomalous westward zonal wind stress and anomalous positive zonal sea level pressure (SLP) gradient to the east at the equator. This change in the zonal SST gradient in the equatorial Indian Ocean is detected even in the lowest-emission scenario, and the size of the change is not necessarily larger in the higher-emission scenario.

With respect to the change over the equatorial Pacific in climate projections, the subsurface central Pacific displays the strongest cooling or weakest warming around the thermocline depth compared to that above and below in all of the climate models, whereas changes in the zonal SST gradient and zonal wind stress around the equator are model dependent and not straightforward.

1. Introduction

It has been decades since global warming became a great matter of concern to people. However, it is still not certain how the climatology of atmospheric and oceanic variables changes in this unprecedented warming.

Earlier studies investigated the response of the tropical Pacific to warming using twentieth-century data records and future climate projections (Cane et al. 1997; Collins et al. 2005; Knutson and Manabe 1995; Liu et al. 2005; Vecchi et al. 2006; Vecchi and Soden 2007). Vecchi et al. (2006) demonstrated a reduction of the zonal sea level pressure (SLP) gradient across the equatorial Pacific by anthropogenic forcing using observational data and model outputs. However, the east–west difference in the response of the equatorial Pacific SSTs to global warming is not clear in both observations and climate projections simulated by coupled general circulation models (CGCMs). Historical SST reconstructions of the twentieth-century demonstrate two contradicting trends regarding the zonal gradient across the equatorial Pacific; SST anomalies based on Rayner et al. (2003) and Kaplan et al. (1998) display a cooling trend in the eastern Pacific throughout the twentieth century, whereas SST anomalies based on Smith and Reynolds (2004) display a warming trend there (see Fig. 17 in Vecchi and Soden 2007). Regarding outputs derived from CGCMs, Collins et al. (2005) found that some CGCMs presented an ''El Niño–like'' SST warming pattern while others exhibited a ''La Niña–like'' pattern; however, most of the CGCMs displayed neither El Niño–like or La Niña–like patterns in the 20 CGCMs conducted with a 1% CO_2 increase scenario. Thus, the response of the zonal SST gradient across the equatorial Pacific to anthropogenic forcing in CGCMs is generally considered to be model dependent (Liu et al. 2005, and references therein).

The response of the tropical Indian Ocean SSTs to global warming in the twentieth-century climate and

* Lamont-Doherty Earth Observatory Contribution Number 7219.

Corresponding author address: Chie Ihara, Lamont-Doherty Earth Observatory of Columbia University, 61 Route 9W, Palisades, NY 10964-8000.
E-mail: cihara@ldeo.columbia.edu

DOI: 10.1175/2008JCLI2581.1

future climate projections is also examined by some studies, but less so compared to the Pacific (Alory et al. 2007; Du and Xie 2008; Ihara et al. 2008; Saji et al. 2006; Vecchi and Soden 2007). Using observational data, Alory et al. (2007) showed that the maximum SST warming in the Indian Ocean between 1960 and 1999 was located around 40°–50°S. Ihara et al. (2008) analyzed observational data throughout the twentieth century and presented a hypothesis on the flattening of the zonal SST gradient across the equatorial Indian Ocean; the climatological gradient that is positive to the east is flattened in the middle of the twentieth century, compared to its state in the late nineteenth century and early twentieth century. They noted that limited data availability in early years hampered the precise discussion on this point. Vecchi and Soden (2007) suggested that the character of the equatorial Indian Ocean's model-simulated response to global warming resembled the positive phase of the Indian Ocean dipole events, though their main subject was the reduction of atmospheric convections under global warming, not the state of the Indian Ocean SSTs in climate projections.

Therefore, it is still important to clearly delineate the change of the climatological, east–west equatorial Indian Ocean SST gradient in global warming and seek an association with changes in other variables obtained from the equatorial Indo-Pacific. Here, a difference in the zonal SST gradient across the equatorial Indian Ocean between the twenty-first-century and twentieth-century climate simulations is presented using the suite of CGCMs participating in the Intergovernmental Panel on Climate Change (IPCC) Fourth Assessment Report (AR4). Based on the idea proposed by Vecchi and Soden (2007), we use the Indian Ocean dipole mode indices in our analysis to represent the condition of the equatorial Indian Ocean. Because earlier studies pointed out that the Indian Ocean dipole mode indices demonstrated strong decadal variability in several CGCMs (Ashok et al. 2004; Song et al. 2007; Tozuka et al. 2007), we compare the centennial state of the index among experiments displaying different warming rates. The change in the equatorial Pacific condition between the twentieth- and twenty-first-century climate simulations is also examined because it is known that the Indian Ocean is not completely independent of the ENSO condition (see section 2 and Table 1).

Section 2 is devoted to descriptions of model outputs used in this study. The Indo-Pacific climate indices calculated from model outputs are described in section 3. In section 4, we assess the statistical significance of the change in the distributions of the Indian Ocean dipole indices between different climate scenarios. In section 5, the response of the annual mean Indo-Pacific Ocean

TABLE 1. Descriptions of models used in this study. Concomitant CCs between September–November (SON) SSTDMI and Niño-3 during the twentieth century are calculated using model outputs based on 20c3m. Further information regarding these CGCMs can be obtained from PCMDI's Web site (online at http://www-pcmdi.llnl.gov/ipcc/model_documentation/ipcc_model_documentation.php).

Modeling groups and model names	Model labels	References	Oceanic horizontal/vertical resolution	Atmospheric horizontal/vertical resolution	CC between SON SSTDMI and Niño-3 in 20c3m
Météo-France, Centre National de Recherches Meteorologiques, CM3	CNRM-CM3	Déqué and Piedelievre (1995)	2° × 0.5° L31	T63 L45	0.20 (0.42 with June–August Niño-3)
CSIRO Atmospheric Research, Australia, Mk3.5	CSIRO Mk3.5	Gordon et al. (2002)	1.875° × 0.84° L31	T63 L18	0.49
National Oceanic and Atmospheric Administration (NOAA)/Geophysical Fluid Dynamics Laboratory, CM2.0	GFDL CM2.0	Delworth et al. (2006)	1° × 1° (1/3°) L50	2.5° × 2° L24	0.55
NOAA/Geophysical Fluid Dynamics Laboratory, CM2.1 Model	GFDL CM2.1	Delworth et al. (2006)	1° × 1° (1/3°) L50	2.5° × 2° L24	0.68
IPSL/Laboratoire de Météorologie Dynamique/Laboratoire des Sciences du Climat et de l'Environnement CM4, version 1	IPSL CM4	Marti et al. (2005)	2° × 1° L31	2.5° × 3.75° L19	0.41
Max Planck Institute for Meteorology, ECHAM5/MPI-Ocean Model (OM)	MPI-OM/ECHAM5	Jungclaus et al. (2006)	1.5° × 1.5° L40	T63 L31	0.50
Meteorological Research Institute, CGCM2.3.2a	MRI CGCM2.3.2a	Yukimoto and Noda (2002)	2.5° × 2.0 (0.5°) L23	T42 L30	0.62
Hadley Centre for Climate Prediction, Met Office, HadCM3	HadCM3	Gordon et al. (2000)	1.25° × 1.25° L30	3.75° × 2.5° L19	0.42

climate to global warming is explored. Section 6 is devoted to a summary and discussion.

2. Data descriptions

The World Climate Research Program's (WCRP's) Coupled Model Intercomparison Project phase 3 (CMIP3) multimodel dataset is used in this study and outputs based on experiments conducted with three different forcing scenarios are analyzed. The first one is the so-called climate of the twentieth-century run (20c3m) that is driven by the estimate of the known historical forcing from 1861 to 2000.[1] The others are two climate projections performed with low- and medium-emission scenarios; the Special Report on Emissions Scenarios (SRES) B1 (B1 is the name used for the experiment forced with this scenario), which is also called the 550-ppm CO_2 stabilization experiment, and SRES A1B (A1B), the 720-ppm CO_2 stabilization experiment (Nakićenović and Swart 2000).

The dipole mode index based on SST anomalies (SSTDMI) represents the difference between the SST anomalies over the western equatorial Indian Ocean (WEIO), from 10°N to 10°S and from 50° to 70°E, and the SST anomalies over the eastern equatorial Indian Ocean (EEIO), from 10°S to the equator and from 90° to 110°E . To represent ENSO, a so-called Niño-3 index is used, defined as SST anomalies in the 5°N–5°S, 150°–90°W box. Indices averaged by the seasons—December–February, March–May, June–August, and September–November—are used in this study.

Saji et al. (2006) has already reported the tropical Indian Ocean variability in the twentieth-century CGCM simulations submitted to the IPCC AR4. Based on their study and our analysis of newly obtained data, we have chosen to work with eight CGCMs that provide all datasets necessary for this analysis and reproduce the observed connection between the interannual variability of the Indo-Pacific Oceans reasonably well (see Table 1 for the details of models analyzed in this study). The eight models chosen demonstrate correlations between the September–November SSTDMI and ENSO index that are comparable to correlations based on observational data, ~0.5,[2] in 20c3m (Table 1). In each CGCM, only one of the ensemble members for an experimental setting is analyzed. Analyses are performed over a 99 yr[3] interval for all experiments, starting from December 1901 and ending at November 2000 in 20c3m, and from December 2001 to November 2100 in the B1 and A1B experiments.[4] Anomalies are calculated using the same climatology regardless of scenarios, the mean of the last 50 yr of the respective 20c3m run. Mostly, comparisons are conducted between outputs based on B1 and 20c3m, but outputs based on B1 and A1B are also compared.

All of the analyzed CGCMs demonstrate that the strongest warming rate of the WEIO SST is in A1B experiment and the weakest is in 20c3m, and the rate of the warming obtained from these forcing scenarios is not very sensitive to which CGCM is used (Table 2).

3. Indian Ocean climate indices in CGCMs

a. *Variability of SSTDMI in climate projections and in 20c3m*

The analysis of the twentieth-century climate simulations in Saji et al. (2006) found that the seasonal dependence of SSTDMI's variability was reasonably simulated. Similarly, variability of SSTDMI is larger in June–August and September–November than in December–February and March–May, in both B1 and 20c3m in all CGCMs used in this study; there is no substantial change in seasonality of SSTDMI's variability in climate projections.

Standard deviations (std devs) of SSTDMI and Niño-3, including all seasons obtained from 20c3m, climate projections, and observations, are summarized in Fig. 1. The warming trend of Niño-3 in climate projections is removed by subtracting the linear best-fit line over the period analyzed. In 20c3m, six CGCMs out of eight have an overactive ENSO (std dev ~ 1–1.5), and two CGCMs, the Meteorological Research Institute Coupled General Circulation Model, version 2.3.2a (MRI CGCM2.3.2a) and the third climate configuration of the Met Office Unified Model (HadCM3), have a weaker ENSO compared to that of the observations (std dev ~ 0.8). All CGCMs demonstrate larger SSTDMI variability in 20c3m (std dev ~ 0.4–0.7) compared to that of the observations (std dev ~ 0.3), except for L'Institut Pierre-Simon Laplace Coupled Model, version 4 (IPSL CM4). This may be partly related to stronger ENSO activities in these models than in the observations. It is interesting that only HadCM3 shows SSTDMI variability that is comparable to that of the Niño-3 variability.

The variance of SSTDMI slightly differs from one experiment to another when forcing scenarios change,

[1] The integration period slightly varies among CGCMs.

[2] The correlation coefficient of September–November Niño-3 with September–November SSTDMI based on the Kaplan SST (Kaplan et al. 1998) is 0.53, and the correlation with SSTDMI based on the ERSST (Smith and Reynolds 2004) is 0.52 during the period from 1900 to 1999.

[3] For MPI/ECHAM5, a 98-yr integration period is analyzed.

[4] Because of the slightly different integration period of each CGCM, the period analyzed varies by about a year or so among CGCMs.

TABLE 2. The warming rate of the WEIO SST in three experiments: SRES A1B, SRES B1, and 20c3m. The warming rates are approximated by the slope of the linear best fit obtained from 10-yr running means of SST anomalies averaged in WEIO.

	Warming per 100 yr [°C (100 yr)$^{-1}$]		
Experiment	20c3m	SRES B1	SRES A1B
CNRM-CM3.0	1.1	1.3	2.7
CSIRO Mk3.5	0.63	1.7	2.6
GFDL CM2.0	0.8	1.4	2.5
GFDL CM2.1	0.7	1.3	2.5
IPSL CM4	0.7	1.8	2.9
MPI-OM/ECHAM5	0.4	2.4	3.6
MRI CGCM2.3.2a	0.8	1.3	2.3
HadCM3	0.56	1.7	2.7

but the difference is significant only in a few cases (see stars in Fig. 1a). Two CGCMs demonstrate a significantly larger Niño-3 variation in B1 compared to its variation in 20c3m, and one model demonstrates a significantly smaller variation in B1 than in 20c3m (Fig. 1b). When comparisons are made between A1B and B1, two CGCMs display significantly larger Niño-3 variations, while two CGCMs have smaller variations.

b. Correlations of SSTDMI with other indices

SSTDMI is diagnostically related to indices based on other oceanic and atmospheric variables, such as sea surface height, SLP, and zonal wind (Yamagata et al. 2002). To confirm the connections of SSTDMI with other variables in warmer climate, correlation coefficients (CCs) between SSTDMI and dipole mode indices based on zonal wind stress and SLP in the three different experimental scenarios are analyzed. The zonal wind stress index[5] (TAUUDMI) represents zonal wind stress anomalies over the equatorial Indian Ocean from 5°N to 5°S, and from 60° to 90°E. The SLP index (SLPDMI) represents the SLP anomaly difference between EEIO and WEIO.[6] A positive TAUUDMI is defined to indicate the presence of westward zonal wind stress anomalies, and a positive SLPDMI is defined to indicate the presence of bigger SLP anomalies over EEIO than over WEIO. The SLPDMI and TAUUDMI that are correlated with observational SSTDMIs are derived from 40-yr European Centre for Medium-Range Weather Forecasts (ECMWF) Re-Analysis (ERA-40) data (Uppala et al. 2005) between 1958 and 2001.

Overall, compared to observational datasets, the coupling between SSTDMI and other dipole indices is stronger in CGCMs (Fig. 2). In 20c3m most models show a strong SST–wind stress–SLP coupling at the interannual time scale (SSTDMI–TAUUDMI CC, ~0.7–0.75, and SSTDMI–SLPDMI CC, ~0.6–0.7), except for Geophysical Fluid Dynamics Laboratory Climate Model version 2.0 (GFDL CM2.0) and IPSL CM4 where the coupling is weaker.

Regarding the change in the strength of the interrelation among the Indian Ocean dipole indices under global warming, CCs of SSTDMI with TAUUDMI–SLPDMI are not significantly different between the B1 and 20c3m experiments or between the A1B and B1 experiments, except for a few cases (see stars in Figs. 2a,b). Therefore, the coupling between SST and wind stress or SLP at an interannual time scale does not change significantly in most cases between B1 and 20c3m experiments, or between A1B and B1 experiments.

The simultaneous relationship between Niño-3 and SSTDMI is model dependent (Fig. 2c). In 20c3m, the strongest association is found in GFDL CM2.1 (CC of 0.46), and the weakest is in GFDL CM2.0 (CC of 0.16). Overall, CCs between SSTDMI and Niño-3 are around 0.3 in 20c3m, which is comparable to the CCs found with observational data. Again, mostly the strength of the connection between SSTDMI and Niño-3 at an interannual time scale does not change significantly from one experimental setting to another (see stars in Fig. 2c).

4. The statistical assessment of the response of the equatorial Indian Ocean climate indices to warming

a. Distributions of SSTDMI during the twentieth and twenty-first centuries

In this section, the significance of the east–west difference in the response of the equatorial Indian Ocean SSTs to global warming is examined by comparing the centennial state of SSTDMI based on experiments of different climate scenarios. Figure 3 displays the cumulative probability density function (CDF) of SSTDMI, including all seasons, during the 99 yr analyzed. The black lines indicate the CDF obtained from SSTDMI based on 20c3m, the red lines are the B1 experiment, and the pink lines are the A1B experiment. Values of SSTDMI in each model are normalized by the standard deviation of SSTDMI derived from 20c3m outputs.

The shape of CDFs differs slightly from one climate model to another. However, in all CGCMs analyzed, CDFs of SSTDMI derived from both B1 and A1B shift to the right, that is, the positive direction, relative to

[5] Saji et al. (1999) originally used zonal wind anomalies to define the dipole mode index.

[6] The SLP-based dipole mode index used here represents SLP anomalies at slightly different locations from the SLP index defined in Yamagata et al. (2002) because it better presents the zonal gradient of SLP at the equator in CGCMs.

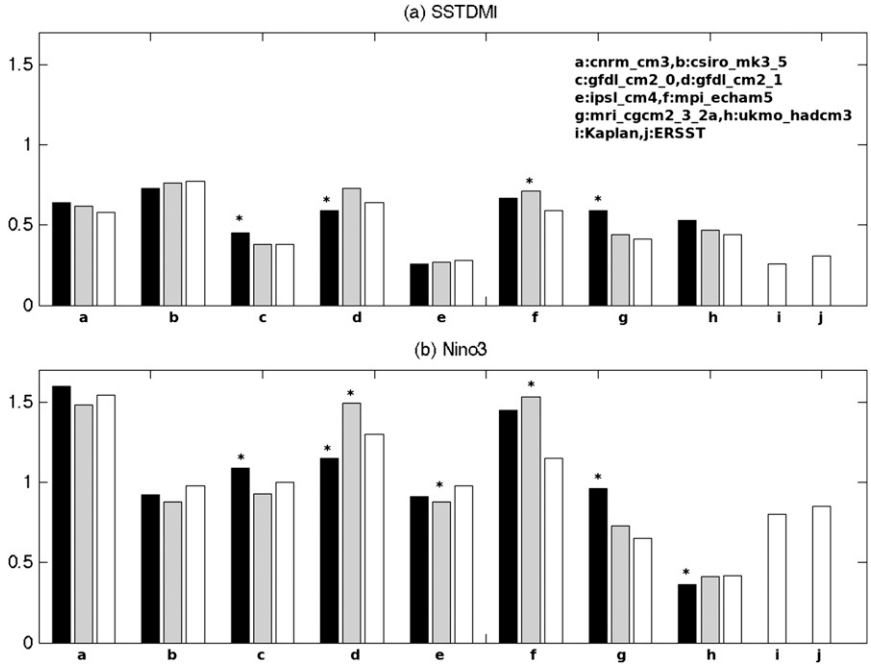

FIG. 1. Standard deviations of SSTDMI and Niño-3 including all seasons for three experiments, SRES A1B, SRES B1, and 20c3m, and observations: (a) SSTDMI and (b) Niño-3; units are °C. The standard deviation based on A1B outputs (black shading), B1 (gray shading), and 20c3m or observations (white). The stars on the top of the bars based on B1 (A1B) outputs indicate that the variation of the corresponding index in B1 (A1B) is significantly different from the variation in 20c3m (B1) at the 95% level and higher. The significance of the difference in two dispersions [the L-scale statistic (Hosking 1990) is used as the test statistics] is assessed using the nonparametric bootstrapping method (Wilks 2006) and a two-sided test is employed.

the CDFs of 20c3m. The significance of the difference between two CDFs is assessed using the two-sample Kolmogorov–Smirnov (KS) test (Table 3). The KS test is more sensitive to the difference in the median than in the extreme values. The difference between CDFs based on 20c3m and B1 is significant at the 94% level or higher in all CGCMs analyzed (Table 3a). Thus, SSTDMI's distribution is significantly shifted to the larger state in B1 than in 20c3m.

It is of interest to see whether a change in CDFs of SSTDMI is larger in the model integration subject to more intense warming scenario. In most models CDFs of SSTDMI based on A1B (the pink lines in Fig. 3) and B1 are almost indistinguishable, and the difference of these CDFs is significant at higher than the 90% level only in two cases (Table 3b). Thus, mostly the size of the shift in SSTDMI's distribution is not very sensitive to the strength of the warming over the Indian Ocean.

The timing of when the SSTDMI shift occurs is model dependent and not clear, particularly in the B1 experiment. Some CGCMs present a clear, positive trend of SSTDMI during the integration period of the B1 experiment; for instance, the Commonwealth Scientific and Industrial Research Organisation Mark version 3.5 (CSIRO Mk3.5) and the Max Planck Institute Ocean Model (MPI-OM)/ECHAM5 display a strong, positive trend in the first half of the twenty-first century, but values of SSTDMI remain the same in the second half of the twenty-first century. While others display both positive and negative trends of SSTDMI during the twenty-first century, SSTDMI values do not change very much in some CGCMs. This may be due to the nature of SSTDMI that shows strong decadal variability. In the A1B experiment, again, the behavior of SSTDMI is model dependent. Some CGCMs display a strong, positive trend of SSTDMI in the first half of the twenty-first century but some show a gradual change toward positive during the entire integration period.

b. Consistency with the shift of other variables

In the previous section, we discuss the change in SSTDMIs in a warmer climate. Interest here is the presence of diagnostic consistency of this shift with the shift of the dipole mode index based on other variables, since the association between SST-based indices and

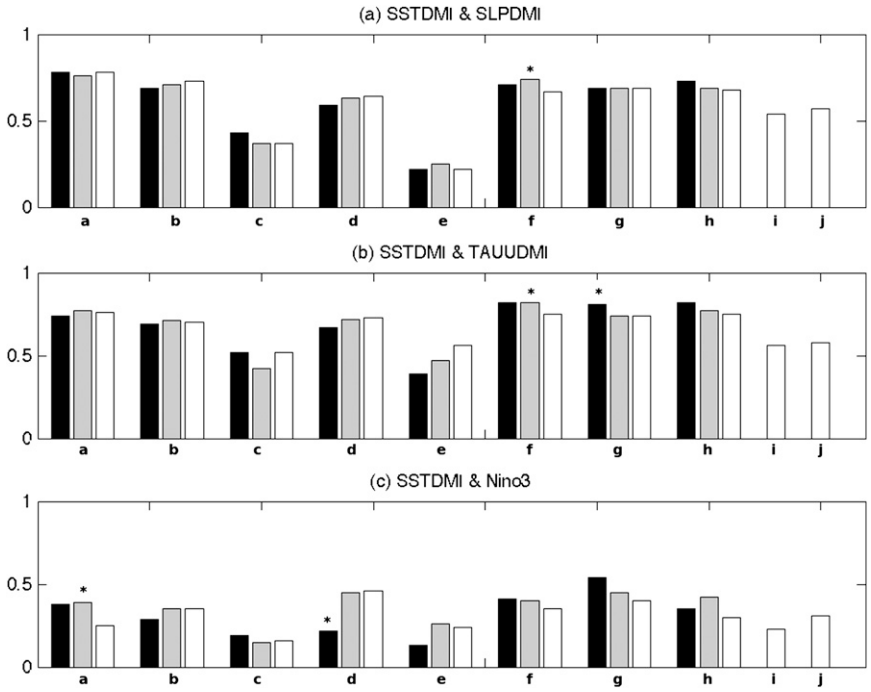

FIG. 2. CCs between SSTDMI and other indices: (a) SLPDMI, (b) TAUUDMI, and (c) Niño-3. The CCs based on A1B outputs (black shading), B1 (gray shading), and 20c3m or observations (white). (a)–(j) Same as in Fig. 1. The stars on the top of the bars based on B1 (A1B) outputs indicate that these CCs are significantly different from the CCs between the same indices in 20c3m (B1) at the 95% level and higher. (The software obtained from http://faculty.vassar.edu/lowry/rdiff.html is used for assessing the significance of the difference in two correlations.) The SLPDMI and TAUUDMI correlated with observational SSTDMIs are derived from ERA-40 data between 1958 and 2001.

zonal wind stress/SLP-based indices has been displayed in section 3.

First, comparisons are made between CDFs of TAUUDMI/SLPDMI based on B1 and CDFs based on 20c3m outputs. CDFs of TAUUDMI derived from B1 shift to the right from CDFs derived from 20c3m, and the difference between these CDFs is significant at the 95% level and higher using two sample KS tests in all CGCMs, except for GFDL CM2.1 (with 84% significance; see Table 3a). Consistent results are obtained from the analysis regarding SLPDMI. CDFs of SLPDMI based on B1 outputs significantly shift to the right from CDFs based on 20c3m outputs in all CGCMs, except for GFDL CM2.1, which shows the shift in the same direction with 88% significance (Table 3a). Therefore, in the B1 experiment, the climatological zonal SST gradient across the equatorial Indian Ocean tends to be anomalously positive to the west compared to the condition in 20c3m, associated with anomalous westward zonal wind stress and an anomalous positive zonal SLP gradient to the east at the equator.

Again, comparisons of CDFs between A1B and B1 are conducted (Table 3b). The size of the change in the CDF of TAUUDMI and SLPDMI is much smaller between B1 and A1B than between B1 and 20c3m. CDFs of TAUUDMI based on A1B outputs do not change significantly from CDFs based on B1 at higher than the 95% level, except for two cases. CDFs of SLPDMI based on A1B significantly shift further to the positive direction relative to those based on B1 in the half of CGCMs analyzed.

5. The change in the tropical Indo-Pacific between B1 and 20c3m experiments

a. The change in annual mean SSTs

Figure 4 shows the difference of the mean Indo-Pacific SSTs in B1 minus the mean in 20c3m including all seasons. It displays the spatial pattern of changes in annual mean SSTs in the B1 experiment compared to that in 20c3m.

1) THE INDIAN OCEAN

Overall, warming is larger in WEIO than in EEIO (Fig. 4), confirming the result based on the examination

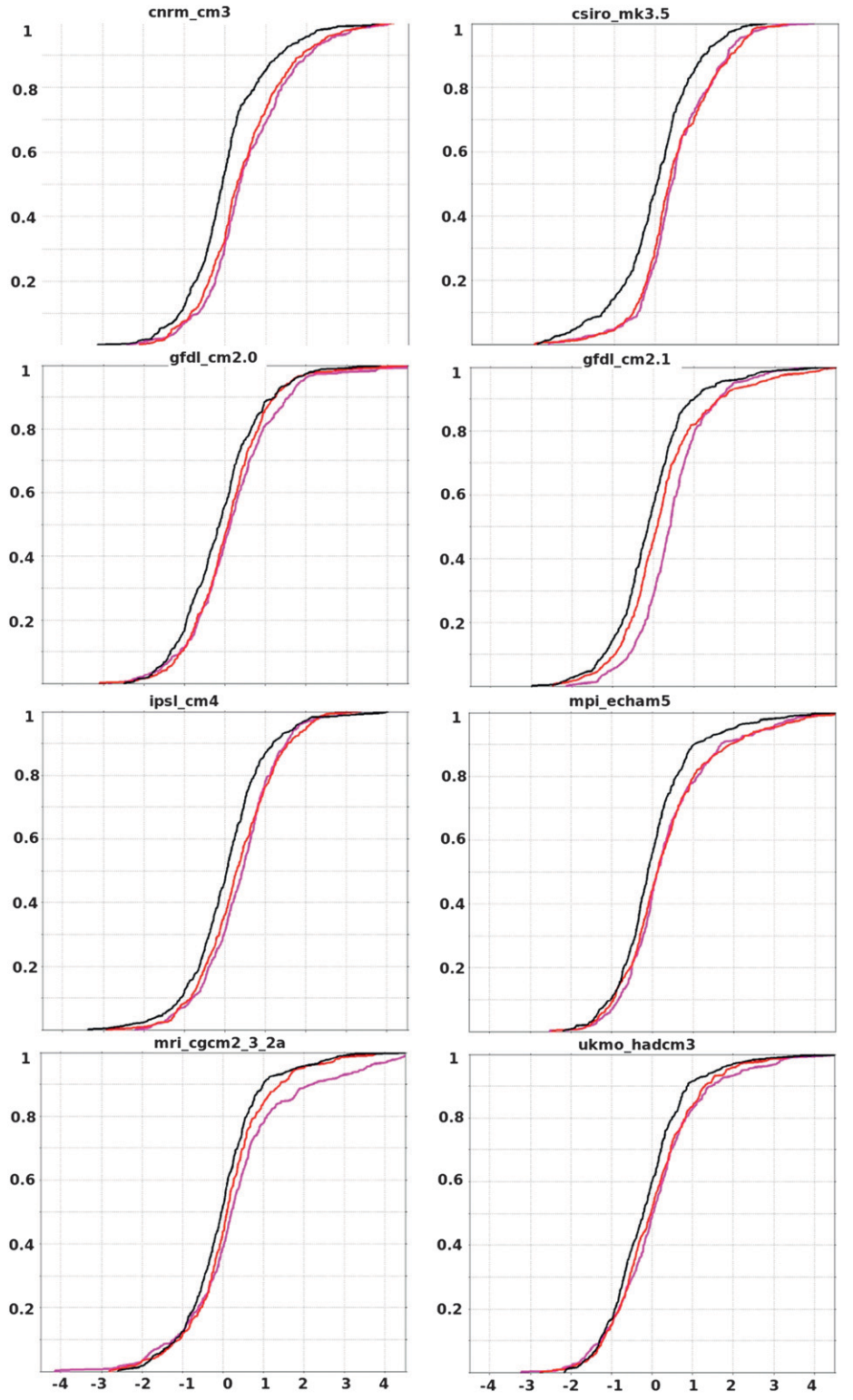

FIG. 3. CFDs of SSTDMI including all seasons; CDFs obtained from 20c3m (black lines), B1 experiment (red lines), and A1B (pink lines). SSTDMIs in 20c3m, B1, and A1B are all normalized by the standard deviation of SSTDMI in 20c3m.

TABLE 3. Significance levels of the difference in CDFs of dipole mode indices obtained from the two sample KS tests: (a) between B1 and 20c3m experimental settings, and (b) between B1 and A1B. The star indicates that the difference in CDFs of two experimental settings is significant at the 95% level and higher. Percent significance is indicated when the significance level is between the 80% and 95% levels. Cells containing no data mean that the significance is below the 80% level.

(a)

CGCM	SSTDMI	TAUUDMI	SLPDMI
CNRM-CM3	*	*	*
CSIRO Mk3.5	*	*	*
GFDL CM2.0	*	*	*
GFDL CM2.1	*	84%	88%
IPSL CM4	*	*	*
MPI-OM/ECHAM5	*	*	*
MRI CGCM2.3.2a	94%	*	*
HadCM3	*	*	*

(b)

CGCM	SSTDMI	TAUUDMI	SLPDMI
CNRM-CM3	—	*	*
CSIRO Mk3.5	—	—	—
GFDL CM2.0	—	—	*
GFDL CM2.1	*	*	80%
IPSL CM4	—	—	—
MPI-OM/ECHAM5	—	90%	88%
MRI CGCM2.3.2a	93%	80%	*
HadCM3	—	—	*

of CDFs derived from SSTDMI. However, when the precise view is taken, the spatial pattern of warming differs from one model to another. The Centre National de Recherches Météorologiques Coupled Global Climate Model, version 3(CNRM-CM3), CSIRO Mk3.5, and GFDL CM2.1 demonstrate a clear east–west contrast in the warming pattern at the equatorial Indian Ocean, whereas in GFDL CM2.0 and HadCM3, the warming in WEIO is evenly spread over the entire basin and the weaker warming is confined in a small region of EEIO.

In CSIRO Mk3.5, the warming pattern is more or less similar to a typical interannual variability pattern of the equatorial Indian Ocean in the 20c3m experiment obtained from the correlation map between the SSTDMI and SST anomalies (Fig. 5). However, most of the models demonstrate broader warming over the entire tropical Indian Ocean in the warming pattern compared to the respective correlation map in 20c3m that shows a strong gradient around the central equatorial Indian Ocean or EEIO.

The difference of the mean zonal wind stress in B1 minus the mean in 20c3m, including all seasons, is negative over the equatorial Indian Ocean (see Fig. 9), and the difference of the mean SLP between B1 and 20c3m in EEIO minus the difference of the mean SLP between B1 and 20c3m in WEIO is positive (figures are not shown for SLP), confirming the result obtained from the analysis regarding CDFs based on TAUUDMI and SLPDMI.

2) THE PACIFIC OCEAN

An overall stronger warming at the equatorial Pacific compared to an around 10°–20° latitudinal band demonstrated by Liu et al. (2005) is consistently presented in outputs analyzed in this study (Fig. 4). In the equatorial Pacific, warming is relatively weaker in the west around the Maritime Continent. When the patterns presented in Fig. 4 are compared to the first EOF of the tropical Pacific SST during 20c3m (Fig. 6), the typical ENSO pattern during the twentieth century simulated by these CGCMs (these ENSO patterns are referred to as El Niño 20c3m), CNRM-CM3, CSIRO Mk3.5, and MRI CGCM2.3.2a demonstrate somewhat similar east–west gradients in the SST warming pattern to that of the zonal gradient pattern found in El Niño 20c3m, though in MRI CGCM2.3.2a a stronger warming spreads farther southward compared to El Niño 20c3m. However, in GFDL CM2.0 and GFDL CM2.1, the central-east equatorial Pacific, around 135°–110°W, demonstrates rather weak warming compared to warming in its east and west sides. In MPI-OM/ECAHM5 and HadCM3, the central equatorial Pacific (the longitudinal band around 170°–140°W) presents weaker warming compared to its east side. IPSL CM4 also demonstrates weaker warming in the central Pacific compared to its west and east sides. Thus, these models display a relatively weaker warming at the central or central-east equatorial Pacific, which is something that is not found in El Niño 20c3m. One of the reasons for this weaker warming might be vigorous equatorial upwelling that inhibits SSTs from warming as proposed by Cane et al. (1997).

A stronger warming in the equatorial Pacific is demonstrated off the west coast of Peru in these CGCMs; however, CGCMs generally have bias in simulating upwelling at the Peruvian coast (Wittenberg et al. 2006), as implied by the fact that the El Niño 20c3m patterns do not show maximum anomalies at the Peruvian coast, unlike the pattern based on the observational datasets. Thus, a definite conclusion regarding the change in SSTs there under global warming, including the effect of coastal upwelling on it, would not be obtained until this bias of CGCMs is solved.

b. The change in annual mean thermocline temperature and zonal wind stress

Figure 7 shows the mean subsurface temperature averaged from 10°S to 0° based on B1 minus the same mean temperature based on 20c3m, including all seasons. The annual mean equatorial temperatures in 20c3m are indicated by the black contours.

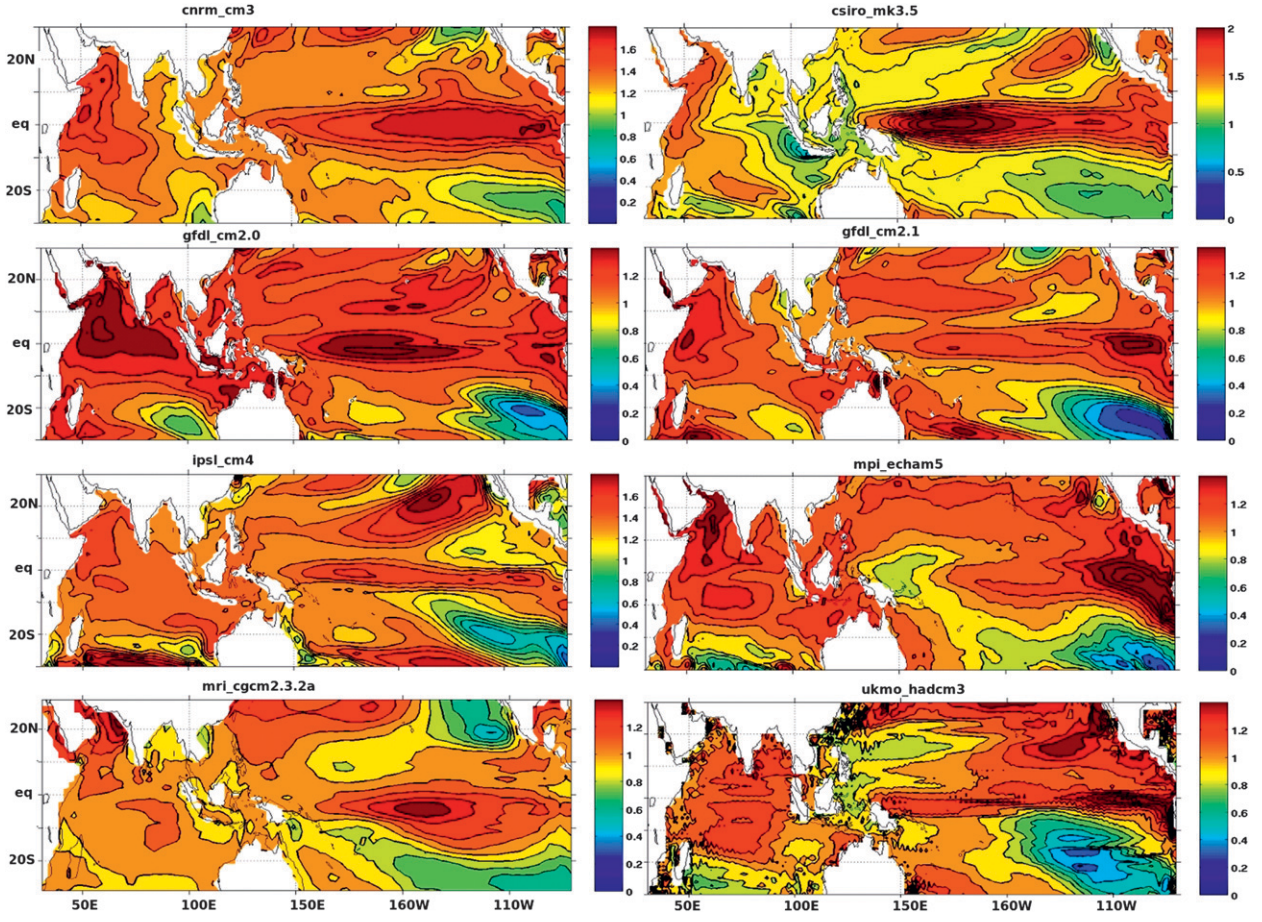

FIG. 4. The difference in the mean Indo-Pacific SSTs based on B1 minus the mean SSTs based on 20c3m including all seasons. Contour intervals are 0.1°C.

EEIO from −50 to −100 m demonstrates less warming compared to the central equatorial Indian Ocean and WEIO at the same depth in all of the CGCMs. This weaker warming in the subsurface EEIO is related to less surface warming in the east compared to that in the west, as we have found in earlier sections. When the comparison is made along the depth in EEIO, the area that roughly corresponds to the thermocline indicated by the climatological temperatures in 20c3m (black contours) shows weaker warming compared to that above and below until ~−150 m in all of the CGCMs, particularly in CNRM-CM3, GFDL CM2.0, MPI-OM/ECHAM5, and MRI CGCM2.3.2a. Below ~−150 m, the size of warming slowly reduces with depth, except for CSIRO Mk3.5, where it remains almost constant. Thus, overall, as pointed out by earlier studies (Alory et al. 2007; Du and Xie 2008; Vecchi and Soden 2007), the CGCM outputs analyzed in this study also show a shoaling of thermocline in EEIO under global warming.

In the Pacific sector, the difference of the mean subsurface temperatures in the western equatorial Pacific between B1 and 20c3m shows cooling in CNRM-CM3, CSIRO Mk3.5, GFDL CM2.0, GFDL CM2.1, MPI-OM/ECHAM5, and MRI CGCM2.3.2a, or weak warming in IPSL CM4 and HadCM3 that contrasts with the strong warming near the surface, and the cooling is strongest (or warming is weakest) around the thermocline depth indicated by the climatological temperatures in 20c3m compared to the depth above and below. Compared to the first EOF of the subsurface temperatures in 20c3m (Fig. 8), the pattern over the equatorial Indo-Pacific associated with El Niño/La Niña 20c3m, the reduction of warming found in EEIO and the western equatorial Pacific in Fig. 7 is somewhat similar to the cooling anomaly pattern associated with El Niño 20c3m in all CGCMs, except for IPSL CM4, which demonstrates only a weak reduction of warming in the subsurface western Pacific. However, at the central or central-east equatorial Pacific the difference in the mean subsurface temperature in B1 minus the mean in 20c3m does not resemble an El Niño 20c3m pattern that demonstrates an anomalous warming there. Overall, cooling or weak

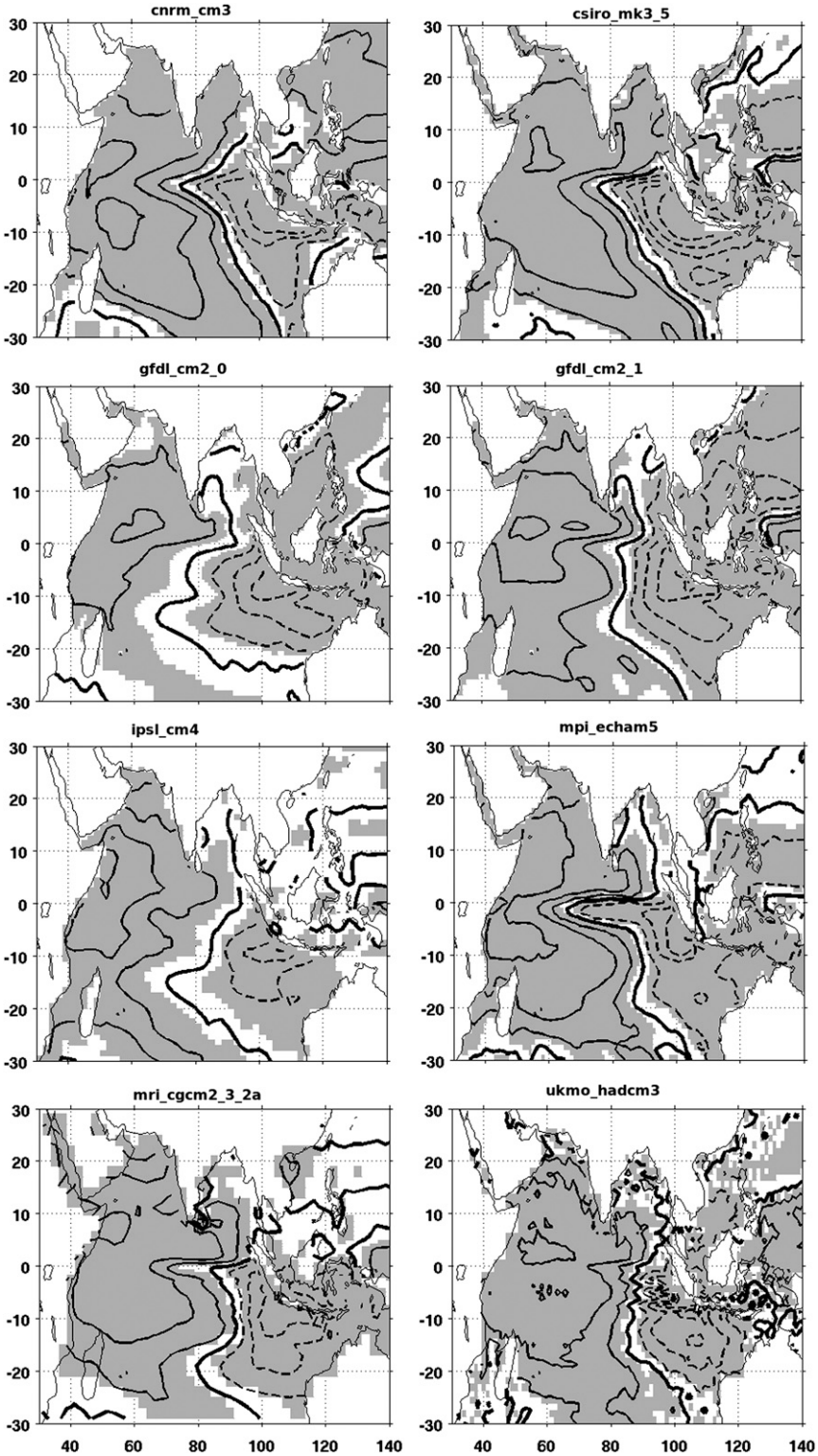

FIG. 5. Correlations between SSTDMI and SST anomalies over the tropical Indian Ocean during 20c3m. Positive (solid lines) and negative values (dashed lines) and the value of 0 (thick solid line) are indicated. Contour intervals are 0.2. Shading indicates that the correlation is significant at 95% level and higher.

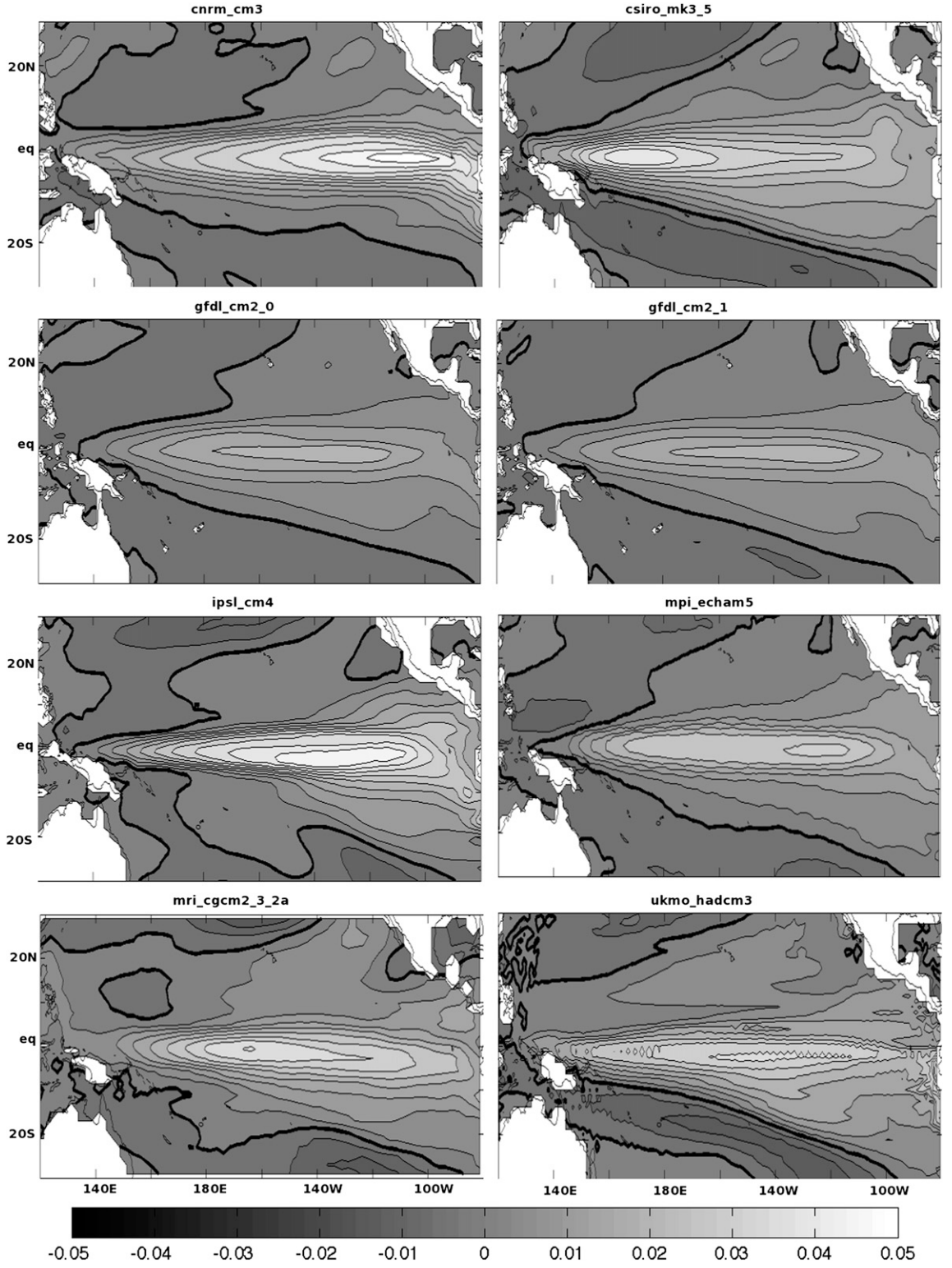

FIG. 6. The first EOF of the Pacific SST anomalies during 20c3m. The linear trend is removed from SST anomalies before calculating EOFs. Value of 0 (thick solid lines) is indicated.

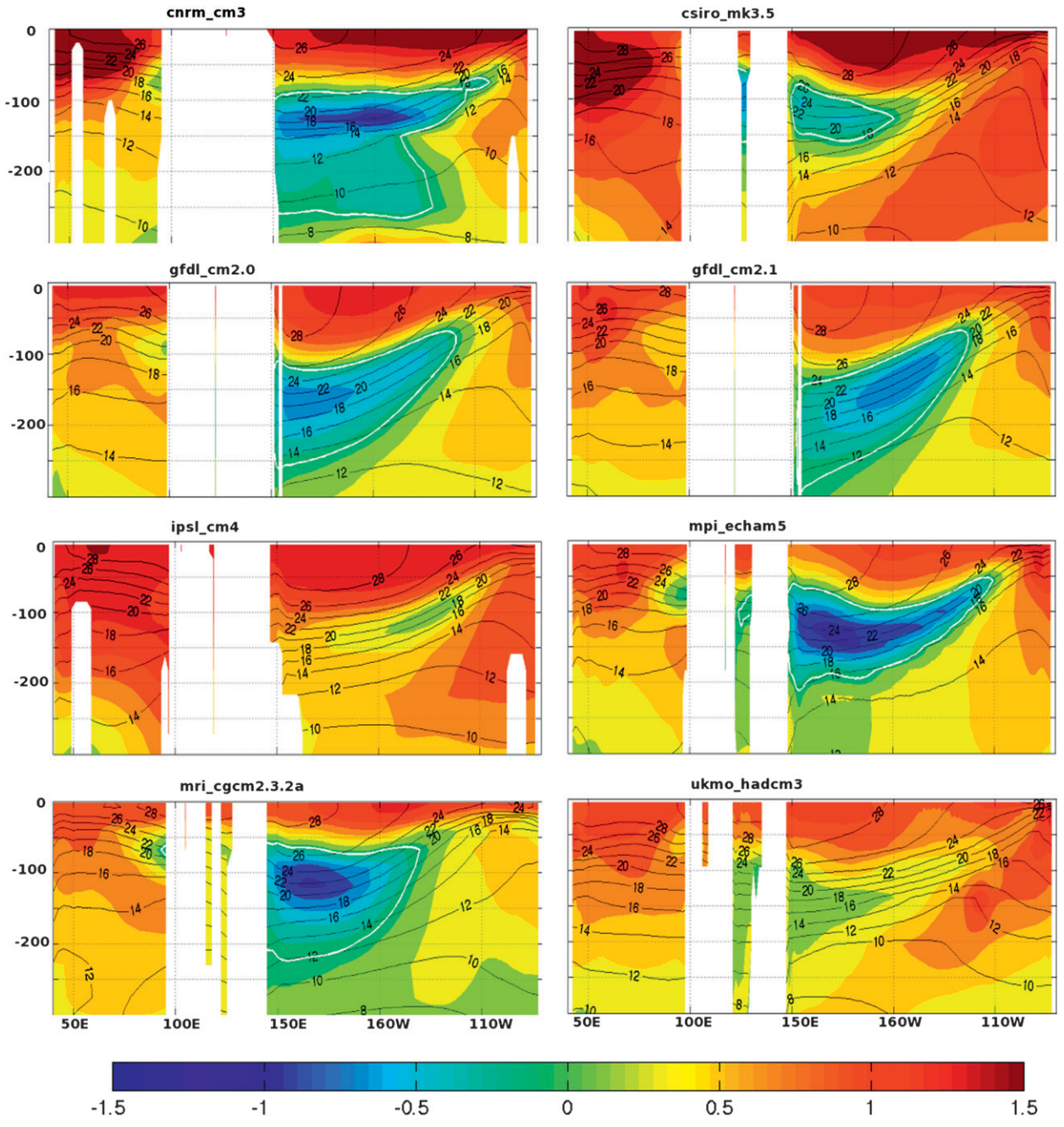

FIG. 7. The annual mean of the longitude–depth section of the equatorial Indo-Pacific temperatures averaged from 10°S to 0° in B1 minus the same mean in 20c3m (shading). Contour intervals for shadings are 0.2°, and 0°C is highlighted by the white contours. The black contours indicate the longitude–depth section of the annual mean potential temperatures in 20c3m. The vertical axis is given in meters.

warming is found around the central equatorial Pacific in Fig. 7, which might explain the weaker SST warming around there demonstrated in some CGCMs. Particularly in GFDL CM2.1, the largest cooling in the difference between B1 and 20c3m is located to the east of 160°W, while the largest cooling anomalies during El Niño 20c3m is located to the west of 160°W.

Thus, similar to results presented by Du and Xie (2008) and Vecchi and Soden (2007), CGCM outputs analyzed in this study also display that the climatological thermocline shoals in almost the entire equatorial Pacific, except for the eastern edge in warmer climate. These studies proposed the reduction of the tropical Walker circulation in climate projections as the reason

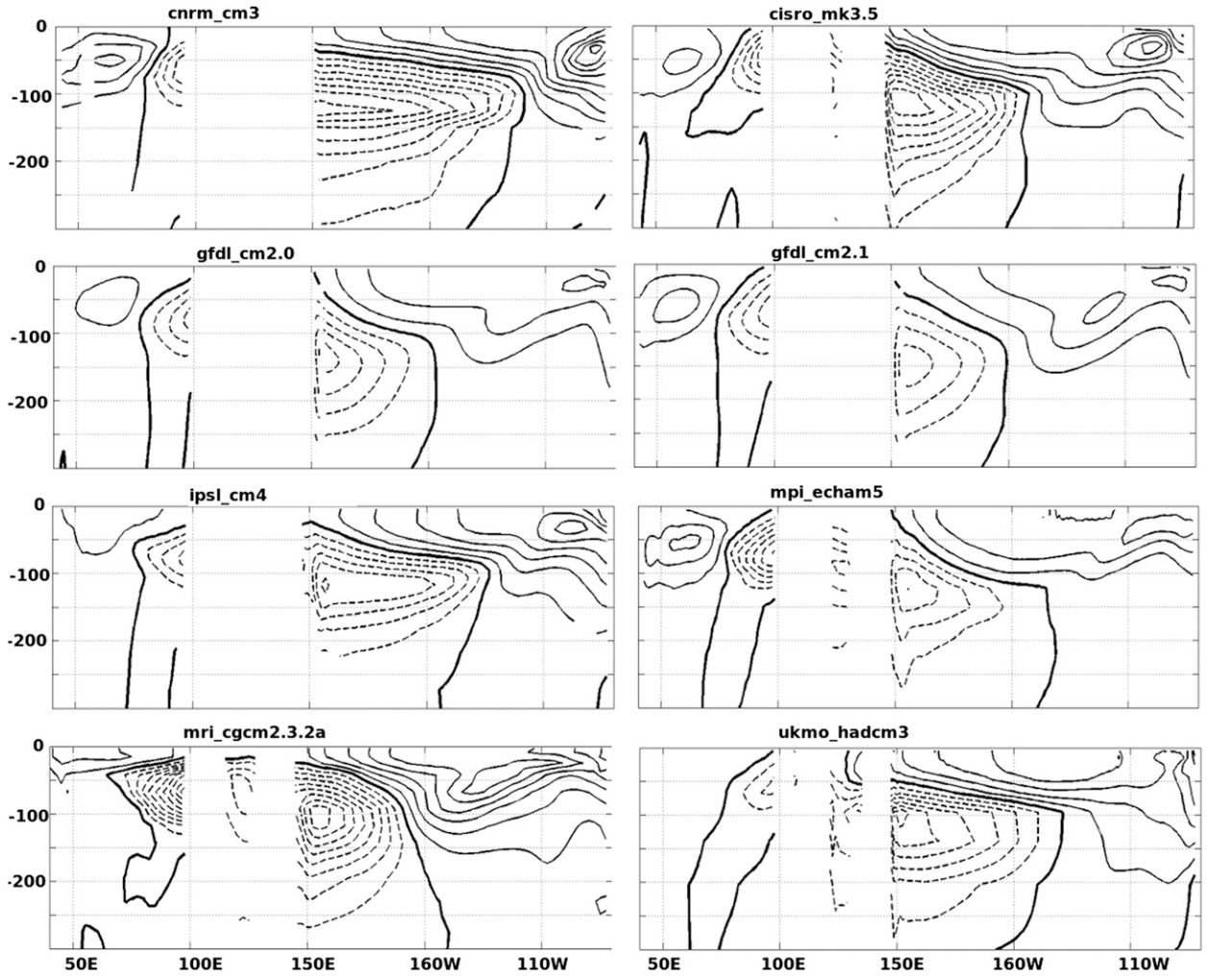

FIG. 8. The first EOF of the longitude–depth section of the equatorial Indo-Pacific potential temperature anomalies averaged from 10°S to 0° during 20c3m. Positive (solid lines) and negative values (dashed lines) and value of 0 (thick solid line) are shown. The vertical axis is given in meters.

for this change in the equatorial Pacific thermocline. However, our analysis of the change in mean zonal wind stress in the following paragraph reveals that the reduction of the tropical Walker circulation is not always found in climate projections and suggests that other factors have affected this change in the equatorial Pacific thermocline.

Figure 9 demonstrates the difference in equatorial mean zonal wind stress in the twenty-first century of the B1 experiment minus the same mean in the twentieth century of 20c3m. While the difference in mean zonal winds is consistently negative over the equatorial Indian Ocean in all CGCMs, it is rather complicated and model dependent over the equatorial Pacific. For instance, a reduction of easterlies over the entire equatorial Pacific is demonstrated in some models, but IPSL CM4 shows an intensification of the equatorial easterlies in warmer climate from 150°E to 110°W. GFDL CM2.1 and HadCM3 shows both reductions and intensifications of easterlies along the equator.

It is speculated that two different processes are involved in the change of the equatorial Pacific thermocline under warming. One is the change of easterlies in the equatorial Pacific; this might be related to the change in the east–west tilt of the thermocline across the equatorial Pacific, and we have found it to be rather model dependent. The other is a diabatic process that affects the change in the mean thermocline depth, the shoaling of the thermocline in the central Pacific that is somewhat similar in all of the models analyzed; in the region where the upwelling is strong, the upwelling could delay warming penetration below the surface mixed layer (Cane et al. 1997), which increases the stratification of the ocean and results in the increase of

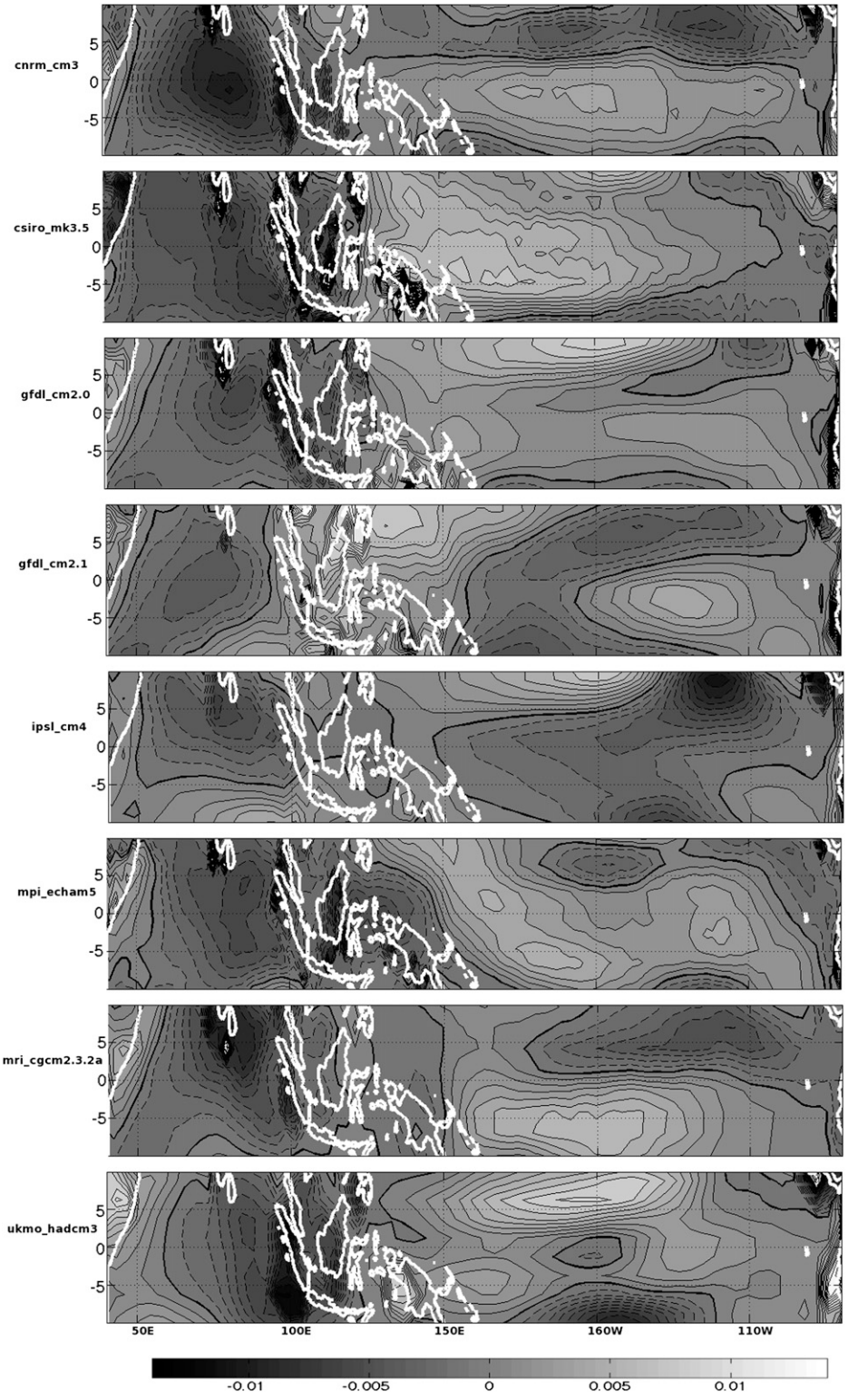

FIG. 9. The difference in mean zonal wind stress based on B1 outputs minus the mean zonal wind stress based on 20c3m. The solid lines indicate positive values, the dashed lines, negative values. The thick solid lines indicate the value of 0. Contour intervals are 0.001 Pa.

the vertical heat advection and cooling/weaker warming around the thermocline in warming climate.

6. Summary and discussion

The response of the equatorial Indo-Pacific Oceans to global warming is investigated using CGCM outputs submitted to the IPCC AR4. CGCMs that are analyzed reasonably well reproduce the features of the SST Indian Ocean dipole mode index in 20c3m and climate projections, SRES B1, and A1B experiments. Our analysis regarding CDFs of SSTDMI reveals that in all climate models analyzed, SSTDMIs are distributed more positively in the twenty-first century B1 scenario than in the twentieth century 20c3m scenario. This shift in CDFs of SSTDMI between B1 and 20c3m settings is consistent with the shift found in CDFs of TAUUDMI and SLPDMI. Thus, we suggest that the climate over the equatorial Indian Ocean is changed under global warming and the zonal SST gradient tends to be less steep in B1 compared to the state in 20c3m, associated with the westward zonal wind stress anomalies and flattened zonal SLP gradient there. Between B1 and A1B experiments, only one climate model demonstrates a significant shift in CDFs of SSTDMI.

As pointed out by earlier studies (Alory et al. 2007; Du and Xie 2008; Vecchi and Soden 2007), in all CGCMs the climatological thermocline depth in EEIO shoals in B1 compared to 20c3m. In the equatorial Pacific, the difference derived from the mean SST in B1 minus the mean SST in 20c3m displays complicated features regarding the east–west gradient and differs from one model to another, as does the change in mean zonal wind stress between these two experiments. Whereas, in all CGCMs studied, the climatological mean thermocline over most of the equatorial Pacific shoals in climate projections, similar to the results presented by Du and Xie (2008) and Vecchi and Soden (2007).

The reduction of the atmospheric convection over the western Pacific warm pool and the increase of SLP there under global warming have been proposed by some studies (Vecchi et al. 2006; Vecchi and Soden 2007). Thus, we speculate that the weaker SST and subsurface temperature warming in EEIO relative to WEIO can be triggered by this change of atmospheric convections under global warming; the anomalously higher SLP over the western Pacific brings about anomalous easterlies over EEIO in climate projections that induce anomalous upwelling and shoal the thermocline there. The weaker warming in EEIO in turn brings about the anomalous positive SST gradient to the west, and thus the anomalous positive SLP gradient to the east across the equatorial Indian Ocean, which makes anomalous easterlies in EEIO that extend farther into the central and western equatorial Indian Ocean. The oceanic connection between the Indo-Pacific basins could also be crucial for the thermocline change in the Indian Ocean under global warming (Cai et al. 2008); the shoaling of the thermocline in the western equatorial Pacific brings about the shoaling of the thermocline in EEIO via the transmission of the interannual time-scale oceanic Rossby wave (Alory et al. 2007) or the reduction of the heat transport at the Indonesian passage in climate projections (Vecchi and Soden 2007).

The shift in CDFs of SSTDMI is found to be significant between B1 and 20c3m in all CGCMs analyzed, but not between B1 and A1B, except for one model. Thus, even the lowest emission scenario is enough to alter the zonal SST gradient in the equatorial Indian Ocean, and the stronger forcing does not increase the size of this shift; whereas the shift in CDFs of SLPDMI between the B1 and A1B scenarios is robust in more CGCMs. It will be interesting to explore whether the diagnostic consistency in the response of the zonal SST gradient and SLP gradient to warming holds when higher emission scenarios are used.

Acknowledgments. We acknowledge the modeling groups for making their model output available for analysis, the Program for Climate Model Diagnosis and Intercomparison (PCMDI) for collecting and archiving this data, and the WCRP's Working Group on Coupled Modelling (WGCM) for organizing the model data analysis activity. The WCRP CMIP3 multimodel dataset is supported by the Office of Science, U.S. Department of Energy. The data portal of the NOAA/Geophysical Fluid Dynamics Laboratory is also acknowledged. CI and VHP were supported under NSF-DMS-0505949. YK and MAC were supported under NA030AR4320179. This work was partly supported by the Columbia University ISE program.

REFERENCES

Alory, G., S. Wijffels, and G. Meyers, 2007: Observed temperature trends in the Indian Ocean over 1960–1999 and associated mechanisms. *Geophys. Res. Lett.,* **34,** L02606, doi:10.1029/2006GL028044.

Ashok, K., W.-L. Chan, T. Motoi, and T. Yamagata, 2004: Decadal variability of the Indian Ocean dipole. *Geophys. Res. Lett.,* **31,** L24207, doi:10.1029/2004GL021345.

Cai, W., A. Sullivan, and T. Cowan, 2008: Shoaling of the off-equatorial south Indian Ocean thermocline: Is it driven by anthropogenic forcing? *Geophys. Res. Lett.,* **35,** L12711, doi:10.1029/2008GL034174.

Cane, M. A., A. C. Clement, A. Kaplan, Y. Kushnir, D. Pozdnyakov, R. Seager, S. E. Zebiak, and R. Murtugudde, 1997: Twentieth-century sea surface temperature trends. *Science,* **275,** 957–960.

Collins, M., and the CMIP Modelling Groups, 2005: El Niño- or La Niña-like climate change? *Climate Dyn.,* **24,** 89–104.

Déqué, M., and J. P. Piedelievre, 1995: High resolution climate simulation over Europe. *Climate Dyn.,* **11,** 321–339.

Dolworth, T. L., and Coauthors, 2006: GFDL's CM2 global coupled climate models. Part I: Formulation and simulation characteristics. *J. Climate,* **19,** 643–674.

Du, Y., and S.-P. Xie, 2008: Role of atmospheric adjustments in the tropical Indian Ocean warming during the 20th century in climate models. *Geophys. Res. Lett.,* **35,** L08712, doi:10.1029/2008GL033631.

Gordon, C., C. Cooper, C. A. Senior, H. T. Banks, J. M. Gregory, T. C. Johns, J. F. B. Mitchell, and R. A. Wood, 2000: The simulation of SST, sea ice extents and ocean heat transport in a version of the Hadley Centre coupled model without flux adjustments. *Climate Dyn.,* **16,** 147–168.

Gordon, H. B., and Coauthors, cited 2002: The CSIRO Mk3 Climate System Model. CSIRO Atmospheric Research Tech. Paper 60, 130 pp. [Available online at http://www.dar.csiro.au/publications/gordon_2002a.pdf.]

Hosking, J. R. M., 1990: L-moments: Analysis and estimation of distributions using linear combinations of order statistics. *J. Roy. Stat. Soc.,* **B52,** 105–124.

Ihara, C., Y. Kushnir, and M. A. Cane, 2008: Warming trend of the Indian Ocean SST and Indian Ocean dipole from 1880 to 2004. *J. Climate,* **21,** 2035–2046.

Jungclaus, J. H., and Coauthors, 2006: Ocean circulation and tropical variability in the coupled model ECHAM5/MPI-OM. *J. Climate,* **19,** 3952–3972.

Kaplan, A., M. A. Cane, Y. Kushnir, A. C. Clement, M. B. Blumenthal, and B. Rajagopalan, 1998: Analyses of global sea surface temperature 1856–1991. *J. Geophys. Res.,* **103,** 18 567–18 589.

Knutson, T. R., and S. Manabe, 1995: Time-mean response over the tropical Pacific to increased CO_2 in a coupled ocean–atmosphere model. *J. Climate,* **8,** 2181–2199.

Liu, Z., S. Vavrus, F. He, N. Wen, and Y. Zhong, 2005: Rethinking tropical ocean response to global warming: The enhanced equatorial warming. *J. Climate,* **18,** 4684–4700.

Marti, O., and Coauthors, 2005: The new IPSL climate system model: IPSL-CM4. Institut Pierre Simon Laplace des Sciences de l'Environment Global Tech. Rep., 86 pp.

Nakićenović, N., and R. Swart, Eds., 2000: *Special Report on Emissions Scenarios*. Cambridge University Press, 570 pp.

Rayner, N. A., D. E. Parker, E. B. Horton, C. K. Folland, L. V. Alexander, D. P. Rowell, E. C. Kent, and A. Kaplan, 2003: Global analyses of SST, sea ice, and night marine air temperature since the late nineteenth century. *J. Geophys. Res.,* **108,** 4407, doi:10.1029/2002JD002670.

Saji, N. H., B. N. Goswami, P. N. Vinayachandran, and T. Yamagata, 1999: A dipole mode in the tropical Indian Ocean. *Nature,* **401,** 360–363.

——, S.-P. Xie, and T. Yamagata, 2006: Tropical Indian Ocean variability in the IPCC twentieth-century climate simulations. *J. Climate,* **19,** 4397–4417.

Smith, T. M., and R. W. Reynolds, 2004: Improved extended reconstruction of SST (1854–1997). *J. Climate,* **17,** 2466–2477.

Song, Q., G. A. Vecchi, and A. J. Rosati, 2007: Indian Ocean variability in the GFDL coupled climate model. *J. Climate,* **20,** 2895–2916.

Tozuka, T., J. J. Luo, S. Masson, and T. Yamagata, 2007: Decadal modulations of the Indian Ocean Dipole in the SINTEX-F1 coupled GCM. *J. Climate,* **20,** 2881–2894.

Uppala, S. M., and Coauthors, 2005: The ERA-40 Re-Analysis. *Quart. J. Roy. Meteor. Soc.,* **131,** 2961–3012.

Vecchi, G. A., and B. J. Soden, 2007: Global warming and the weakening of the tropical circulation. *J. Climate,* **20,** 4316–4340.

——, ——, A. T. Wittenberg, I. M. Held, A. Leetmaa, and M. J. Harrison, 2006: Weakening of tropical Pacific atmospheric circulation due to anthropogenic forcing. *Nature,* **441,** 73–76, doi:10.1038/nature04744.

Wilks, D. S., 2006: *Statistical Methods in the Atmospheric Sciences*. 2nd ed. Academic Press, 627 pp.

Wittenberg, A. T., A. Rosati, N.-C. Lau, and J. J. Ploshay, 2006: GFDL's CM2 global coupled climate models. Part III: Tropical Pacific climate and ENSO. *J. Climate,* **19,** 698–722.

Yamagata, T., S. K. Behera, S. A. Rao, Z. Guan, K. Ashok, and H. N. Saji, 2002: The Indian Ocean dipole: A physical entity. *CLIVAR Exchanges,* No. 24, International CLIVAR Project Office, Silver Spring, MD, 15–18.

Yukimoto, S., and A. Noda, 2002: Improvements in the Meteorological Research Institute Global Ocean-Atmosphere Coupled GCM (MRI-CGCM2) and its climate sensitivity. Japan National Institute for Environmental Studies Tech. Rep. 10, 8 pp.